

Membrane based Deformable Mirror: Intrinsic aberrations and alignment issues

A. Raja Bayanna,^{1,*} Rohan E. Louis,² S. Chatterjee,³

Shibu K. Mathew,¹ and P. Venkatakrishnan¹

¹*Physical Research Laboratory, Udaipur Solar Observatory, Udaipur-313034, India.*

²*Leibniz-Institut für Astrophysik Potsdam (AIP),
An der Sternwarte 16, 14482, Potsdam, Germany*

³*Indian Institute of Astrophysics,
Koramangala, Bangalore-560017, India and
BGVS, Indian Institute of Science Campus, Bangalore, 560012, India*

Abstract

A Deformable Mirror (DM) is an important component of an Adaptive Optics system. It is known that an on-axis spherical/parabolic optical component, placed at an angle to the incident beam introduces defocus as well as astigmatism in the image plane. Although the former can be compensated by changing the focal plane position, the latter cannot be removed by mere optical re-alignment. Since the DM is to be used to compensate a turbulence-induced curvature term in addition to other aberrations, it is necessary to determine the aberrations induced by such (curved DM surface) an optical element when placed at an angle (other than 0 deg) of incidence in the optical path. To this effect, we estimate to a first order, the aberrations introduced by a DM as a function of the incidence angle and deformation of the DM surface. We record images using a simple setup in which the incident beam is reflected by a 37 channel Micro-machined Membrane Deformable Mirror for various angles of incidence. It is observed that astigmatism is a dominant aberration which was determined by measuring the difference between the tangential and sagittal focal planes. We justify our results on the basis of theoretical simulations and discuss the feasibility of using such a system for adaptive optics considering a trade-off between wavefront correction and astigmatism due to deformation.

OCIS codes: (220.1080) Active or adaptive optics; (220.1140) Alignment; (220.1010) Aberrations (global); (220.1000) Aberration compensation.

<http://dx.doi.org/10.1364/XX.99.099999>

* bayanna@prl.res.in

1. Introduction

It is known that the most important component of an Adaptive Optics (AO) System is the corrector, which is the Deformable Mirror (DM). It can be a continuous face sheet or a surface formed by mirror segments [1]. In the former the mirror boundary is fixed and voltage applied to any one actuator influences the neighbouring surface as well. In the case of the Micro-machined membrane Deformable Mirror(MMDM) [2] this influence can be as large as 60% [3]. However, they are still preferred in many AO systems [4-8] because of their low cost and capability of achieving large stroke. A 37 channel MMDM from OKOTECH, Netherlands, is being used by us at the Udaipur Solar Observatory (USO) for its solar adaptive optics [9-11] (SAO) system. Although the MMDM is not common in many SAO systems, its performance has been validated for solar observations[12].

In an AO system, it is necessary to bias the DM in such a way that the stroke can be achieved in both positive and negative directions from the biased position. In general, this can be achieved by applying a constant voltage to all the actuators. In case of the MMDM, application of a constant voltage to all the actuators deforms the mirror to a shape often approximated to be parabolic [13]. However, such approximations do not hold, at points away from the centre. A DM, whose surface is distorted by applying a uniform set of voltage to its actuators, and placed in the optical setup at an angle to the beam will undoubtedly mimic a tilted parabolic mirror. Such a tilted curved/parabolic mirror will induce optical aberrations such as defocus, astigmatism and coma [19]. While defocus can be compensated by moving the imaging system, astigmatism and coma cannot be corrected by a simple alignment. As the DM is also being used to compensate a turbulence-induced curvature term, it is necessary to determine the maximum angle of incidence at which the DM can be placed in the optical setup without introducing an additional set of aberrations

than that which are inherent to the DM. Otherwise, at relatively large angles of incidence, when the DM corrects an atmosphere-induced defocus (curvature term), it will inevitably introduce astigmatism. In order to minimize this astigmatism, an additional correction is required. This constraints the bandwidth of the system.

Along with ‘setup’ induced aberrations, intrinsic aberrations (aberrations due to mirror’s surface profile) are also very important. As the technical passport of the DM states that the initial figure of the DM is astigmatic upto 1.3 fringes(P-V)[14], we would like to study the intrinsic aberrations as well.

In this paper we estimate, to a first order, the aberrations introduced in the optical system as a result of folding the beam using a DM with a bias voltage, for various angles of incidence. The rest of the paper is organized as follows. Section 2 describes theoretical aspects related to the deformation of the mirror under an external, uniform voltage and in section 3 we present the theoretical investigation on astigmatism and defocus in such a deformed system. Section 4 describes the simulations which demonstrate the aberrations introduced when the DM is placed at different angles of incidence. The degradation in the observed image quality with varying curvature for different angles of incidence is discussed in Section 5 using an experimental setup. The understandings from the simulations and the observations from the experiment are discussed in Section 6.

2. Theoretical perspective of the deformable mirror under the influence of voltage

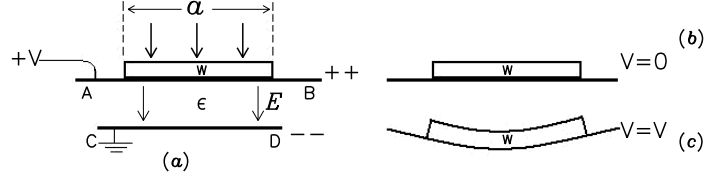


Fig. 1. Schematic of the membrane surface. W is the wafer surface, a is the diameter of the surface and ϵ is di-electric constant. d is the distance between the electrodes AB and CD. Thickness of the wafer is h .

In Figure 1, the silicon wafer W , with upper surface polished is place on the +ve electrode AB, which is subjected to potential V , while the -ve electrode CD is grounded. When $V = 0$, the wafer W has its undistorted shape (b), while it gets distorted to the shape, shown in (c), when $V \neq 0$. If d be the separation between the plates and ϵ be the dielectric permittivity of the material, filling the space between the plates, a charge density $\Sigma = \epsilon V/d$ develops on the plates. The resulting stress is given by

$$P = \epsilon V^2 / (2d^2) \quad (1)$$

Thus, if E be the young's modulus, σ be the Poisson ratio and h be the thickness of the wafer, then the deformation of the upper surface of the wafer is given by[18]

$$z(x, y) = \frac{-3P(1 - \sigma^2)}{128 Eh^3} [a^2 - (x^2 + y^2)]^2 \quad (2)$$

$$\text{for } x = y = 0, \quad z(0, 0) = -\frac{P}{64} \frac{3(1 - \sigma^2)}{2 Eh^3} a^4 = -h_0 \quad (3)$$

where h_0 is defined as the sag of the membrane.

The gradient of the surface at any point on the (x, y) membrane are given by

$$\begin{aligned} z_x &= \partial z / \partial x = \frac{4h_0}{a^4} x [a^2 - (x^2 + y^2)] \\ z_y &= \partial z / \partial y = \frac{4h_0}{a^4} y [a^2 - (x^2 + y^2)] \end{aligned} \quad (4)$$

Accordingly, the two curvatures are given for $z_x, z_y \ll 1$

$$\begin{aligned} K_x &= \frac{1}{\rho_x} = -\frac{\partial^2 z}{\partial x^2} = -\frac{4h_0}{a^4} [a^2 - 3x^2 - y^2] \\ K_y &= \frac{1}{\rho_y} = -\frac{\partial^2 z}{\partial y^2} = -\frac{4h_0}{a^4} [a^2 - x^2 - 3y^2] \end{aligned} \quad (5)$$

The convention being that the curvature is positive if the surface is convex (center of curvature is located at $z < 0$ i.e below the undistorted surface) and negative if the surface is concave (center of curvature is located at $z > 0$ i.e above the undistorted surface). where, ρ_x and ρ_y are the radii of curvature along x - and y - direction respectively. The point where K_x or K_y or both equal to zero indicates the point of inflexion. Thus, at the center $x = y = 0$, $\rho_x(0, 0) = -a^2/4h_0 = \rho_y(0, 0) = \rho_0$ and we can express the equation (2) as

$$z(r) = -h_0 + \frac{r^2}{2\rho_0} - \frac{r^4}{4\rho_0 a^2} \quad (6)$$

where, $r^2 = x^2 + y^2$. In the literature, the formula that is traditionally used for the radius of curvature is $R = (a^2/2h_0 + h_0/2)$. This gives a value, which is much larger than the actual radius of curvature at the center, it's magnitude being ρ_0 . This is because on these formula, the circumference of the mirror ($x^2 + y^2 = a^2, z$) and the point of sag ($x = 0 = y, z = -h_0$) are fitted to lie on a sphere for which simple geometry gives a radius R as given above. The actual values are, however given by equation 5, showing that the surface cannot be described by a unique radius of curvature. The various aberrations, which appear in the Fraunhofer limit are thus to be worked out with $z(x, y)$ being given by equation 2, in which $z(x, y)$ is found to be proportional to V^2 , a fact, which we present in our further results.

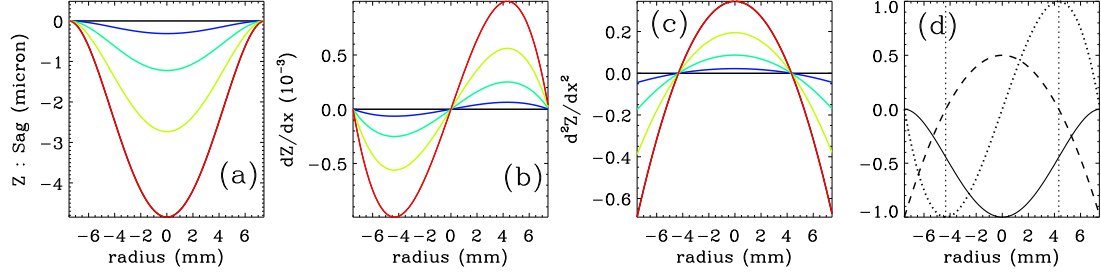


Fig. 2. (a) Surface elevation $z(x,0)$ (b) gradient $z_x(x,0)$ and (c) curvature of the membrane at different points along the diameter for application of different voltages from 0 to 200 V; (d) elevation $z(x,0)$, (continuous line), gradient (dotted line) and curvature (dashed line), for the application of 200 volts; vertical dotted lines show the points of inflexion. Different parameters for a typical wafer that are being used here are: $E = 165 \text{ GPa}$, $\sigma = 0.24$, $h=2.5 \text{ } \mu\text{m}$, $a=7.5 \text{ mm}$. The colors in plots (a-c), black, blue, green, yellow and red represent for voltages 0, 50, 100, 150, and 200 V, respectively.

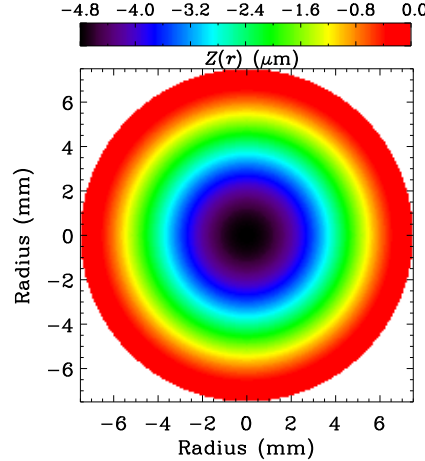


Fig. 3. Surface map of the membrane with the application of a voltage of 200 V. We fit this surface with first 21 Zernike polynomials; Z4(defocus) and Z11(Spherical aberration) are the dominant terms.

Figure 2 show typical manifestations of z , inclination and curvature of the membrane and the location of inflexion for typical values of various parameters of equation 2. It is clear that the variations in Z_x and Z_y at different points on the surface, imply a reflecting surface with varying inclination, which would, in geometrical viewpoint, reflect the light from these points of incidence in different directions, consistent with the laws of reflection. The curvatures K_x and K_y ascribe focusing and defocusing properties of the reflecting membrane surface. Figure 3 show the surface map of the membrane with the application of voltage; we fitted this surface with 21 Zernike polynomials [16], the retrieved coefficients show that the $Z4$ (defocus) and $Z11$ (spherical aberration) are the dominant terms.

3. Image formation by a deformable mirror

Figure 4 illustrates the image formation by a DM. We assume that the DM lies in the xy plane in its un-deformed state, and the curved profile DD_1D_2 represents the DM under the influence of uniform voltage. The deformation $z(x, y)$ follows the equation (6) given in section 2. Let a ray from a point source $P_1(-X_1, Y_1, Z_1)$ be incident on the curved mirror at $P(x, y, z(x, y))$. The light ray reflected by the DM is imaged using a lens of focal length f_0 on to a screen ‘S’ placed at a distance of Z_f from the lens. The lens lies in the $\chi\eta$ plane such that $\chi\eta\zeta$ form a right handed system of orthogonal axes. The lens introduces a path length ‘Lens’ to the ray on propagating through the lens.

In order to find the path followed by the rays, we calculate the path length P_1PQP_2 and minimize the same with respect to (x, y) and (χ, η) as demanded by Fermat’s principle. The total optical path is given by

$$L_{tot} = P_1P + PQ + QP_2 + \text{Lens} \quad (7)$$

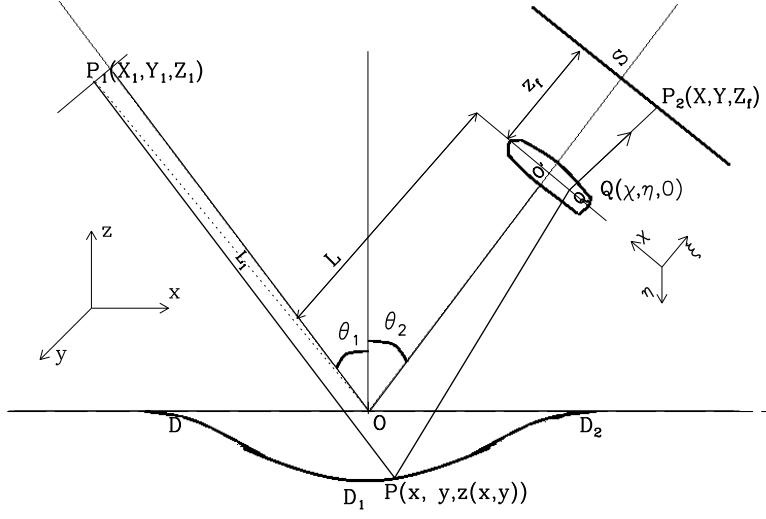


Fig. 4. Ray diagram for image formation due to deformable mirror

For a perfectly aligned optical system, we have $\theta_1 = \theta_2$, so that

$$L_{tot} = \frac{\alpha_{11}}{2}x^2 + \frac{\alpha_{22}}{2}y^2 + \frac{\beta_{11}}{2}(\chi^2 + \eta^2) + \frac{\beta_{22}}{2}(X^2 + Y^2) + \gamma_{11}x\chi + \gamma_{22}y\eta + \delta_o(X\chi + Y\eta) \quad (8)$$

where, $\alpha_{11} = \cos \theta_1 [\cos \theta_1 / L - 2 / \rho_o]$

$$\alpha_{22} = 1/L - 2 \cos \theta_1 / \rho_o$$

$$\beta_{11} = 1/L + 1/Z_f - 1/f_0$$

$$\beta_{22} = 1/Z_f$$

$$\gamma_{11} = -\cos \theta_1 / L,$$

$$\gamma_{22} = -1/L, \quad \delta_o = -1/Z_f \quad (9)$$

Here, we have neglected the terms contributing to a constant phase and kept only the leading terms that contribute to astigmatism and defocus. In order to find the path of the ray we apply Fermat's principle. Thus keeping (X, Y) fixed we minimize L_{tot} w.r.t x, y, χ, η respectively, to yield,

$$\begin{aligned}
\alpha_{11} x + \gamma_{11} \chi &= 0 \\
\alpha_{22} y + \gamma_{22} \eta &= 0 \\
\gamma_{11} x + \beta_{11} \chi + \delta_o X &= 0 \\
\gamma_{22} y + \beta_{11} \eta + \delta_o Y &= 0
\end{aligned} \tag{10}$$

which are linear equations in the variables x, y, χ, η, X, Y . Solving the above linear equations,

$$\begin{aligned}
\chi &= -(\alpha_{11}/\gamma_{11}) x, \\
\eta &= -(\alpha_{22}/\gamma_{22}) y \\
X &= \left[(\alpha_{11}\beta_{11} - \gamma_{11}^2)/(\gamma_{11}\delta_o) \right] x = \alpha x \\
Y &= \left[(\alpha_{22}\beta_{11} - \gamma_{22}^2)/(\gamma_{22}\delta_o) \right] y = \beta y
\end{aligned} \tag{11}$$

here, the definitions for α, β can be found from the pre-factors. These equations relate $(x, \chi, X; y, \eta, Y)$ with each other. In other words, if the diameter of the lens be much larger than $2a$, i.e. the diameter of the DM then for any point of incidence $(x, y, z(x, y))$ on the DM, we know the point (X, Y, Z_f) , which the ray of light reaches.

On defining $\tan \theta = (x/y)$ we can write the coordinates of the point (x, y) on the DM to be $x = r \cos \theta$ and $y = r \sin \theta$. Thus, various rays, incident on the circle: $x^2 + y^2 = r^2$ on the DM, will reach the point $(X(r), Y(r), Z_f)$, where $X(r) = \alpha r \cos \theta$, and $Y(r) = \beta r \sin \theta$. This means that $(X(r), Y(r))$ describes an ellipse $(X(r)/\alpha r)^2 + (Y(r)/\beta r)^2 = 1$. Thus on making $r = a$ we find all rays will reach (X_m, Y_m, Z_f) where on the screen all the rays will lie inside a ellipse (X_m, Y_m) such

that

$$X_m = \alpha a \cos \theta, \quad Y_m = \beta a \sin \theta \quad (12)$$

$$(X_m/\alpha a)^2 + (Y_m/\beta a)^2 = 1 \quad (13)$$

The results given in (12) and (13) enable us to estimate the astigmatic aberration inside the system.

3.A. Location of the Astigmatic foci

Consider a case where on adjusting the screen and making $Z_f = f_0 + \delta_1$ we can make $\alpha = 0$. In this case, $X_m = 0$ the illumination on the screen will be confined only along the Y axis. The necessary condition for that, i.e $\alpha = 0$ requires $\alpha_{11} \beta_{11} = \gamma_{11}^2$, as seen from equations (11). Then on using the definition given in equation (9), we find in the limits $|\delta_1/f_o| \ll 1$ and $\rho_0 \ll 2L$,

$$\begin{aligned} \delta_1 &= -(2/\rho_0 \cos \theta_1) f_0^2, \\ Z_f = f_1 &= f_0 + \delta_1, \\ &= f_0 - (2f_0^2/\rho_0 \cos \theta_1) \end{aligned} \quad (14)$$

Similarly on adjusting $Z_f = f_0 + \delta_2$ we can make $\beta = 0$. In this case $Y_m = 0$ and the illumination on the screen is confined only along the axis. For this to happen, we must have $\alpha_{22}\beta_{11} = \gamma_{22}^2$ so that for $|\delta_2/f_o| \ll 1$, we get on using the definitions in equations (9),

$$\begin{aligned} \delta_2 &= -(2 \cos \theta_1/\rho_0) f_0^2, \\ Z_f = f_2 &= f_0 + \delta_2, \\ &= f_0 - (2 \cos \theta_1 f_0^2/\rho_0) \end{aligned} \quad (15)$$

The astigmatism in the system is then estimated as

$$\begin{aligned}\delta f &= f_1 - f_2 = -2 f_0^2 \sin^2 \theta_1 / \rho_0 \cos \theta_1 \\ &= \frac{-2 f_0^2}{\rho_0} f(\theta_1) \propto V^2 \theta_1^2\end{aligned}\quad (16)$$

The above equation for astigmatism (δf) shows a strong dependence on θ_1 , it varies very fast for $\theta_1 \geq 60^\circ$ and blows up as $\theta_1 \rightarrow 90^\circ$ (c.f. Table 1). It also shows that δf varies as V^2 .

3.B. Location of circle of least confusion

For any value of $Z_f = f_0 + \Delta$ the patch of light on the screen lies inside an ellipse, defined by equations (12) and (13). Thus, the extent of the patch is defined by averaging $R_m^2(\theta) = X_m^2(\theta) + Y_m^2(\theta)$ over $0 \leq \theta \leq 2\pi$. These give,

$$\begin{aligned}\overline{R_m^2(\theta)} &= \overline{X_m^2(\theta)} + \overline{Y_m^2(\theta)} \\ &= \alpha^2 a^2 \overline{\cos^2 \theta} + \beta^2 a^2 \overline{\sin^2 \theta} \\ &= \frac{a^2}{2} [\alpha^2 + \beta^2]\end{aligned}\quad (17)$$

The circle of least confusion is located at a point, where $\overline{R_m^2}$ is minimum, i.e. at a value of Δ for which,

$$\frac{d}{d\Delta} \overline{R_m^2} = 0 = \frac{a^2}{2} \left[2\alpha \frac{d\alpha}{d\Delta} + 2\beta \frac{d\beta}{d\Delta} \right] \quad (18)$$

These derivatives can be evaluated from equations (11) on using the definitions given in equation (9). We find that in the limit $\rho_0 \cos \theta_1 \rightarrow \infty$, i.e. for curvatures not too large, as is the case for most practical situations.

$$\Delta \approx -(4f_0^2/\rho_0) F(\theta_1) \propto V^2 F(\theta_1) \quad (19)$$

$$\text{where, } F(\theta_1) = \frac{\cos \theta_1}{1 + \cos^2 \theta_1} \quad (20)$$

Table 1. Dependence of circle of least confusion on angle of incidence

θ_1	0	15	30	45	60	75	90
$f(\theta_1)$	0.000	0.069	0.288	0.707	1.500	3.605	∞
$F(\theta_1)$	0.500	0.499	0.495	0.471	0.400	0.242	0

We find that $F(\theta_1)$ varies very slowly with θ_1 until θ_1 exceeds 60° . Beyond this the condition of large $\rho_0 \cos \theta_1$ may breakdown and the above approximation is no longer valid. Variation of $F(\theta_1)$ with respect to θ_1 is shown in Table 1. However for low values of θ_1 the point of least confusion shifts as given by equation (20), being quadratic in V and weakly dependent on θ_1 . The results given above are tested by simulation and experimentally and are described in the subsequent sections.

It is to be noted that in our analysis we have kept in Eq.(8) terms which are up to the second order in x , y , χ , η , X , and Y . Extending to a higher order, there appears a term $2(\chi X + \eta Y)(X^2 + Y^2)/Z_f^3$ in L_{tot} that is ascribed to aberration due to coma, which we neglected in our analysis for the following reason.

The extra term gives rise to additional terms linear in X and Y in the last two equations of Eq.(10). These additional terms are smaller than the last terms in these equations ($\delta_0 X$ and $\delta_0 Y$ respectively, with $\delta_0 = 1/Z_f$) by a factor, which is of the order of $(a/Z_f)^2 \approx 1.4 \times 10^{-3}$ as can be seen with $a = 7.5$ mm and $Z_f \approx f_0 = 200$ mm as is the case in our system. This smallness of coma in comparison to astigmatism is also borne out by the results displayed in Table 3.

4. Simulations

The simulations were carried out using *ZEMAXTM* [15], an optical design software to study the influence of voltage on the DM kept at an angle to the incident beam. The simulations were performed for the DM with and without any intrinsic surface figure.

4.A. Simulations without any intrinsic aberrations

Figure 5 describes the two optical configurations (OC) where the DM is placed at 0° (OC-1) and 45° (OC-2) to the incident collimated beam, respectively. The radius of curvature (ρ_0) of the DM is related to its radius (a) and sag (h_0) by the relation

$$\rho_0 = \frac{a^2}{4h_0} = \frac{256}{3\epsilon(1-\sigma^2)} \frac{h^3 d^2}{a^2 V^2} \propto \frac{1}{a^2 V^2} \quad (21)$$

The radius of curvature (ρ_0) was calculated for voltages from 0 to 225 volts in steps

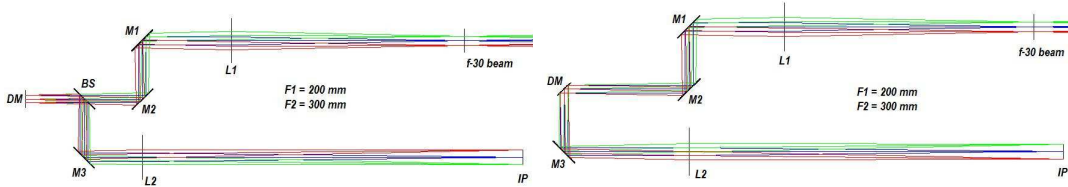


Fig. 5. Optical layouts of the two configurations; Left: configuration-1, Right: configuration-2. An Input beam of F#30 was collimated by a lens of focal length 200 mm. M1 and M2 are steering mirrors, one of them was used as Tip-tilt mirror (TTM). DM was placed at the pupil plane. The collimated light was focused using a lens (L2) of focal length of 300 mm, which gives a plate scale of 30.5 arc-sec/mm at the image plane (IP). In configuration-1, one of the reflected beams from beam splitter (BS) is not shown here.

Table 2. Aberration coefficients of Configuration-OC1. The Zernike coefficients before and after correspond to the cases when a voltage was applied to the DM that was then followed by shifting the focal plane during the aberration minimization scheme.

Voltage	Sag	ρ_0	Defocus	Zernike Coefficients				WFE (λ)	
V	(μm)	(m)	(mm)	Z4	$Z_{11} \times 10^{-5}$			Before	After
				Before	After	Before	After		
				$\times 10^{-5}$				$\times 10^{-4}$	
0	0.00	∞	0	0	0	0	0	0	0
25	0.07	187.6	001.71	0.07	0.4	0.21	0	0.07	0.06
50	0.30	46.90	006.85	0.28	1.6	0.84	0	0.28	0.24
75	0.67	20.84	015.50	0.63	3.6	1.87	0	0.63	0.55
100	1.20	11.72	027.77	1.12	6.4	3.28	0	1.12	0.97
125	1.87	07.50	043.82	1.75	10.0	5.02	0	1.75	1.52
150	2.70	05.21	063.86	2.52	14.4	7.01	0	2.52	2.18
175	3.67	03.83	088.20	3.43	19.6	9.17	0	3.43	2.97
200	4.80	02.93	117.18	4.47	25.6	11.35	0	4.47	3.89
225	6.07	02.31	151.25	5.66	32.3	13.35	0	5.66	4.93

of 25 volts. It is to be noted here that the user manual supplied by the manufacturer of the DM states that the maximum central deflection of the DM surface is $7 \mu\text{m}$. As a result, the f-number of the DM varies from infinity to ≈ 67 . The final wavefront quality of the system was estimated by assigning the values of ρ_0 to the DM in OC-1 and OC-2. In OC-1, application of voltage to DM (i.e. RC to DM) causes only defocus error, whereas in case of OC-2, it also causes astigmatism in addition to defocus. We estimated the aberration coefficients in terms of Zernike coefficients.

Table 3. Aberration coefficients of Configuration-OC2

Voltage (V)	Defocus (mm)	Zernike Coefficients						WFE (λ)	
		Z4		Z6		$Z7 \times 10^{-4}$		Before	After
		Before	After	Before	After	Before	After		
		$\times 10^{-4}$							
0	0	0	0	0	0	0	0	0	0
25	01.18	0.07	0.11	0.035	0.035	0.01	0.008	0.08	0.04
50	07.27	0.29	0.44	0.139	0.139	0.18	0.137	0.33	0.14
75	16.45	0.67	0.99	0.315	0.315	0.92	0.694	0.74	0.32
100	29.49	1.19	1.77	0.559	0.559	2.92	2.193	1.31	0.56
125	46.56	1.85	2.76	0.874	0.874	7.13	5.353	2.05	0.87
150	67.91	2.67	3.97	1.259	1.259	14.8	11.10	2.95	1.26
175	93.88	3.63	5.39	1.714	1.714	27.4	20.57	4.02	1.71
200	124.8	4.75	6.99	2.238	2.238	46.7	35.08	5.25	2.24
225	161.4	6.00	8.76	2.833	2.833	74.9	56.20	6.65	2.83

In OC-1, the dominant aberration is defocus ($Z4$) along with a negligible amount of spherical aberration($Z11$) of the 3rd order (Table 2). These aberrations increase with the increase in voltage as seen from their corresponding Zernike coefficients (cf., Table 2). To compensate these aberrations the focal plane position must be shifted which is achieved by minimizing the merit function for an optimal focal plane position in ZEMAX. The process of optimization yields a wavefront error which is well within the diffraction limit.

In OC-2, the dominant aberrations were defocus ($Z4$), astigmatism ($Z6$) along with small amounts of coma ($Z7$) (Table 3). These aberrations also increase with an

increase in voltage. After optimizing the focal plane position, the Z4 coefficient reduces considerably, while the coefficient Z6, namely astigmatism, remains unchanged. The overall wavefront quality varies from $\lambda/12.5$ to 6.6λ when the voltage changes from 25-225 V, before optimization. After optimization the values vary from $\lambda/25$ to 2.83λ for the same range of voltage. Thus at an angle of incidence of 45° , application of any voltage to the DM introduces an additional astigmatism and coma (cf., Table 3). It is to be noted that here the coefficient of coma is very small in comparison to that of astigmatism. Hence, we neglect coma in our further analysis. However, we conjecture that the coefficient of coma is negligible because of the large f-number of the curved DM mirror, this may not be the case with a tilted curved mirror with a smaller f-number, where the coma is equally important as astigmatism [19].

As a further step, the amount of astigmatism induced by the (curved) DM for different angles of incidence was studied, as it is the only term that remains unaltered after optimization. As a matter of convenience the astigmatism is expressed as the change in tangential and sagittal focal planes rather than Zernike coefficients as these values can be compared with those from an optical setup having a test target. Figure 6 shows the increase in astigmatism (change in sagittal and tangential focii) with increase in voltage (i.e decrease in RC) for different angles of incidence. Dependence of astigmatism and defocus on voltage and angle of incidence is derived empirically. It shows that defocus depends only on the voltage applied, whereas astigmatism depends both on the voltage applied and the angle of incidence. This is in agreement with the theory (cf., equations 16 and 19). Similarly, the wavefront error of the system at optimum focus varies with angle of incidence and it shows a similar trend as astigmatism. The system shows a considerable amount of WFE for angles of incidence $\theta_i \geq 9^\circ$, with the WFE is worse than $\lambda/10$ for any voltage.

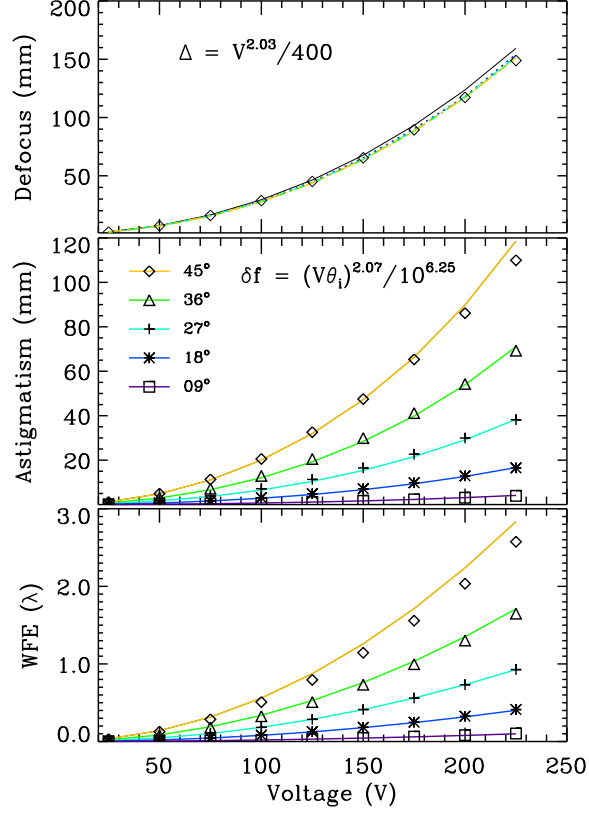


Fig. 6. Top panels show amount of focus shift needed to minimize the aberrations with the application of voltage at various angles of incidence. Middle panels show the change in the amount of astigmatism with the applied voltage for different angles of incidence (θ_i). Bottom panels: Wavefront error (WFE) after optimization for optimum focus. Relation between applied voltage and astigmatism and defocus are shown in the respective figures. The symbols represent the fitted values based on relations derived empirically.

4.B. Simulations with intrinsic astigmatism

The technical document of the DM states that in the absence of any voltage the initial mirror figure is astigmatic upto 1.3 fringes. In the simulations, this intrinsic

aberration was modeled by utilizing "Zernike Fringe Sag" [17]. The terms Z5, Z6 and, Z12, Z13 refer to the first and third order astigmatism, respectively and were adjusted such that the initial difference between the tangential and sagittal focus was 6 mm which corresponds to a wavefront error of 0.18λ at $\lambda = 550$ nm. The obtained coefficients were assigned to the DM to make the surface astigmatic. The entire exercise as described in Section 4.A was repeated, astigmatism and wavefront error were estimated for different angles of incidence. At an angle of incidence of 0° , the wavefront error remains constant at 0.18λ after optimizing the focal plane for different values of RC, which correspond to the intrinsic astigmatism. At any other angle of incidence the wavefront error shows quadratic variation with the increase in RC with a minimum value being around 0.18λ . This shows that the astigmatism arising from the surface figure needs to be corrected before using the DM in an optical setup.

5. Experiment

5.A. Optical Setup

To compare the results from the ZEMAX simulations, we carried out an experiment with the DM, using an F#15 Coude telescope as the light feed. With a set of relay lenses the image was magnified by a factor of 2. At the focal plane of the F#30 beam an artificial target was placed which was illuminated by sunlight. A lens of focal length 200 mm was used to collimate the light modulated by the target. The DM was placed in the collimated beam which reflects the beam towards an imaging lens of focal length 300 mm (refer figure 5). The voltage to the DM was controlled by 2, 8-bit PCI cards whose maximum output voltage to any channel is 5 V. The individual actuators were first assigned a port address as stated in the user

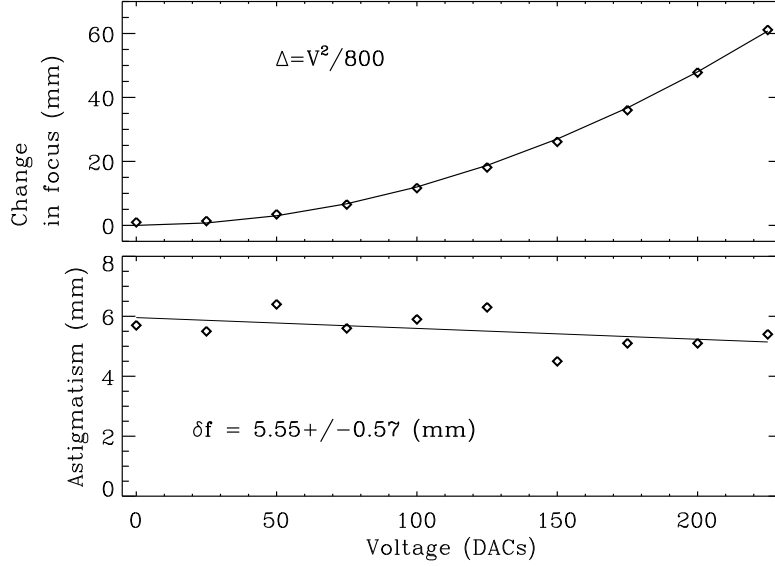


Fig. 7. Defocus and astigmatism when the DM is kept at angle of incidence of 0° . Top panel show change in focus w.r.t change in voltage. Bottom panel show Intrinsic astigmatism, as there is no tilt in the DM, astigmatism observed is intrinsic to the DM. Solid line represents the linear fit corresponds to the data points.

manual and the PCI output was checked for each channel. A high voltage amplifier consisting of 2 high voltage amplifier boards, boost the signal from the PCI cards. Each amplifier board contains 20 non-inverting DC amplifiers with a gain of 59. A high voltage stabilized DC supply was used to power the amplifier boards. The maximum operating voltage of the DM is 162 V which corresponds to 256 Digital-to-Analog Counts (DAC). A 1392×1024 pixel, Cool-Snap HQ CCD with a pixel size of $6.45 \mu\text{m}$ from Roper Scientific was used to image the target. The difference between tangential and sagittal planes and the circle of least confusion (optimum focus) were measured in order to estimate the intrinsic as well as induced aberrations.

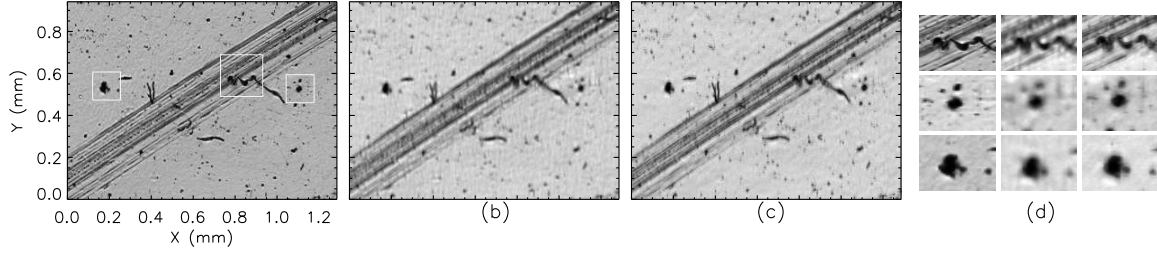


Fig. 8. Image quality (a) due to plane mirror (along with three features identified for further processing), contrast = 1, (b) due to DM (plane mirror replaced by a DM), contrast = 0.6, (c) after applying some correction to DM, contrast = 0.64. (d) Three rows corresponds to three features identified in (a) shown in white boxes; along the row the images are due to plane mirror, DM and correction respectively; contrast improvement varies from 4% to 10%. The scale shown is in mm.

5.B. Intrinsic aberrations and Image quality

For measuring the intrinsic aberration the DM was placed at an angle of 0° similar to OC-1 in Figure 5. The target had an L shape pattern and it was observed that the vertical line was focused at one location while the horizontal line at another. This difference in the sagittal and tangential focus is caused by astigmatism. To see if this astigmatism changes with the curvature of the DM, a uniform voltage was applied to all 37 actuators of DM from 0 to 225 DACs in steps of 25 DACs. For every voltage set, the tangential, sagittal and optimum focal positions (f_1 and f_2) were measured and the corresponding images were recorded. The difference between the sagittal and tangential focal positions do not vary with voltage (cf., Figure 7) which is in agreement with the results from the theory and simulation when an intrinsic astigmatism is considered for 0° angle of incidence. The optimum focus changes quadratically with the voltage applied.

The presence of an intrinsic astigmatism results in a poor image quality which can

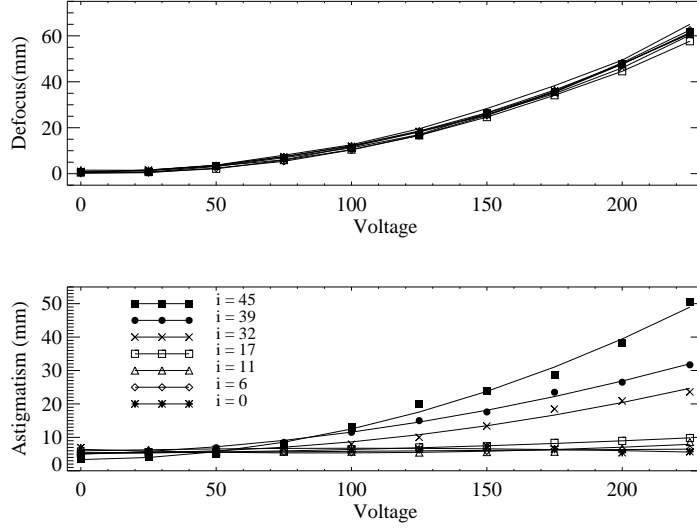


Fig. 9. Top panel shows the change in focal plane (circle of least confusion) with the increase in voltage (in DACs). Bottom panel shows astigmatism with increase in in voltage (in DACs) for different angles of incidence.

be judged visually as shown in Figure 8 which also shows images taken by a plane mirror kept at the same location of the DM. Astigmatism essentially arises due to different curvatures along different directions, hence as a first order trial we applied maximum voltage to a specific line of actuators alone and recorded the corresponding image as shown in Figure 8c. As a performance measurement, contrast of the images was estimated before and after correction for the entire image as well as for a few selected features as shown in Figure 8d. Although the improvement in image contrast is nominal, it is evident that a specific voltage set is necessary to compensate for the degradation caused by the intrinsic astigmatism.

The experiment was repeated by placing the DM at several angles of incidence and the tangential, sagital and optimum focus positions (f_1 and f_2) were measured and the corresponding images were also recorded. The defocus is quantified by noting the

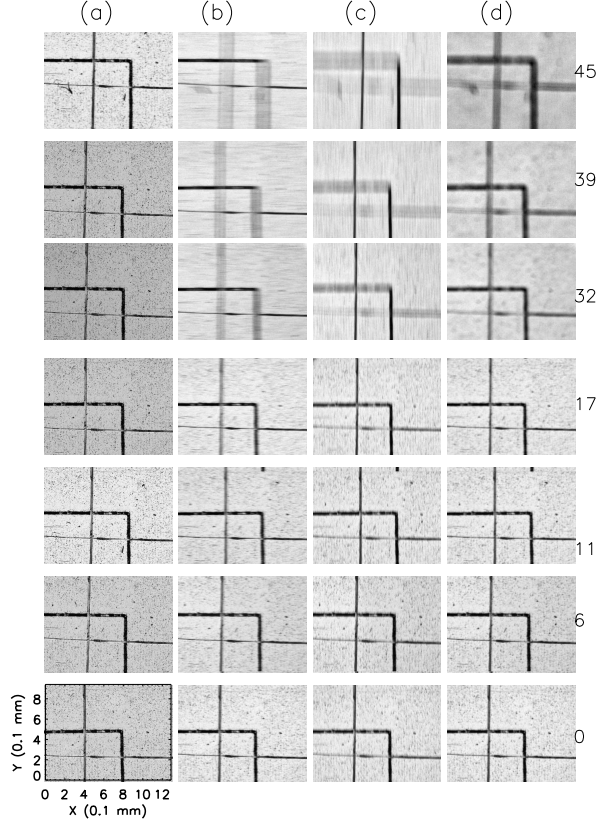


Fig. 10. Images at 225 DACs to all actuators of DM for different angles of incidence (a) due to plane mirror, (b) due to DM at sagittal plane (c) due to DM at tangential plane (d) due to DM at the plane of least confusion. The images are of size 300×220 pixels² with a scale of 4.3 micron per pixel.

distance Δ by which the screen has to be shifted to reach the position of the circle of least confusion. The astigmatic aberrations is quantified by $\delta f = |f_1 - f_2|$. Both Δ and δf are proportional to V^2 , their dependence on θ_1 are strikingly different as seen from equations 16 and 20. While the defocus Δ has a weak dependence on θ_1 , that of δf has a strong dependence on θ_1 as seen from the functional forms of $F(\theta_1)$ and $f(\theta_1)$.

The results are displayed in Figure 9 which is in agreement with those from the theory and simulations. Interestingly, for angles less than 10° the astigmatism remains nearly a constant with the applied voltage as seen from the theory and simulations. Images obtained for different angles of incidence by applying 225 DACs to all the actuators of DM are shown in Figure 10.

6. Discussion and conclusions

A deformable mirror is an important component in an adaptive optics system for compensation of atmospheric turbulence. A simple optical setup was made to study alignment issues and the intrinsic aberrations of a deformable mirror without employing any kind of wavefront sensor.

The nature of the surface deformation under the influence of a uniform voltage to all the actuators of deformable mirror is obtained theoretically and given in equation (2). The equation is used to calculate the sag of the deformed/curved mirror. It is shown that radius of curvature of the deformable mirror is inversely proportional to the square of the voltage applied. Furthermore, we also analytically estimated the defocus and astigmatism due to such a curved mirror, which are shown in equations (16) and (20).

Simulations were performed with different voltages to the deformable mirror, which is kept at different angles of incidence. It is demonstrated that the estimated error in focus is solely a function of the applied voltage where the former has a quadratic dependence on the latter. The same is seen in astigmatism as well with an additional non-linear dependence on the angle of incidence. Simulations also shows that coefficient of coma is negligible in comparison to astigmatism, could be due to the large f-number of DM.

Similar results were obtained from the experiment, wherein a 37 channel MMDM

is placed in the collimated beam at different angles of incidence. The DM when placed at 0° angle of incidence shows a finite amount of intrinsic astigmatism which does not vary significantly with the radius of curvature (i.e. application of voltage to DM); this is in agreement with the technical report provided by the manufacturer. It is also observed that the optimum focal plane position changes quadratically with voltage and does not exhibit a change of sign which concludes that the DM does not possess any intrinsic curvature that would change sign on application of voltages. We have also shown that the image quality degrades with the application of voltage and the astigmatism increases with the increase in angle of incidence.

From both, simulations and experiment it is demonstrated that when the DM is kept at angles greater than 0° and voltages are applied to it, there is an induced astigmatism which increases in general with the angle of incidence as is also predicted by the theory. The close correlation between theory and experiment enable us to reach the following conclusion about the performance of DM. It shows that apart from the forces appearing due to charging of the capacitor, there are no other spurious deforming forces in the system and the optics of the DM can thus be regarded to have sufficient reliability. The detailed intensity distribution on the screen can also be computed by using equation (9) for the phase distortion due to deformation.

It is concluded that in order to operate the DM in real-time to correct for atmospheric induced aberrations, it necessary to a) keep the DM at a very small angle of incidence and b) to derive a suitable voltage set that will compensate the intrinsic astigmatism as well. This voltage set can be simply added to any constant voltage set required to bias the DM surface, since the intrinsic astigmatism is independent of voltage; it naturally facilitates using a suitable bias voltage in order to allow the membrane to move in either direction, which is being pursued and will be reported in future.

In practical situations, for wavefront correction the deformation may not be as

simple as considered in the present investigations. However, the present study enables us to ascertain the inherent defects in the system which has to be kept in mind, while using the deformable mirror for phase distortion correction.

Rohan E. Louis is grateful for the financial assistance from the German Science Foundation (DFG) under grant DE 787/3-1 and the European Commission's FP7 Capacities Programme under Grant Agreement number 312495.

References

- [1] M. C. Roggeman, B. M. Welsh, and R. Q. Fugate, "Improving the resolution of ground-based telescopes", *Rev. Mod. Phys.* **69**, 438-505 (1997).
- [2] Ende Li, Yun Dai, Haiying Wang, and Yudong Zhang, "Application of eigenmode in the adaptive optics system based on a micromachined membrane deformable mirror", *Appl. Opt.* **45**, 5651-5656 (2006).
- [3] Gleb Vdovin and P. M. Sarro, "Flexible mirror micromachined in silicon", *Appl. Opt.* **34**, 2968-2972 (1995).
- [4] Lijun Zhu, Pang-Chen Sun, Dirk-Uwe Bartsch, William R. Freeman, and Yeshaiah Fainman, "Adaptive Control of a Micromachined Continuous-Membrane Deformable Mirror for Aberration Compensation", *Appl. Opt.* **38**, 168-176 (1999).
- [5] D. S. Dayton, S. Restaino, J. Gonglewski, J. Gallegos, S. MacDermott, S. Browne, S. Rogers, M. Vaidyanathan, and M. Shilko, "Laboratory and field demonstration of a low cost membrane mirror adaptive optics system", *Opt. Commun.* **176**, 339-345 (2000).
- [6] C Paterson, I Munro and J C Dainty, "A low cost adaptive optics system using a membrane mirror", *Optics Express*, **6**, 175-186 (2000).
- [7] Enrique J. Fernandez, Ignacio Iglesias, and Pablo Artal, "Closed-loop adaptive optics in

- the human eye”, Opt. Lett. **26**, 746-748 (2001).
- [8] Eirini Theofanidou, Laurence Wilson, William J. Hossack and Jochen Arlt, “Spherical aberration correction for optical tweezers”, Opt. Comm. **236**, 145-150 (2004).
 - [9] Thomas R. Rimmele, “Solar adaptive optics”, in *Adaptive Optical Systems Technology*, Peter L. Wizinowich, ed., Proc. SPIE **4007**, 218-231 (2000).
 - [10] Oskar van der Luehe, Dirk Soltau, Thomas Berkefeld, and Thomas Schelenz “KAOS: Adaptive optics system for the Vacuum Tower Telescope at Teide Observatory” in *Innovative Telescopes and Instrumentation for Solar Astrophysics*, Stephen L. Keil, Sergey V. Avakyan, ed., Proc. SPIE **4853**, 187-193 (2003).
 - [11] Goran B. Scharmer, Peter M. Dettori, Mats G. Lofdahl, and Mark Shand, “Adaptive optics system for the new Swedish solar telescope” in *Innovative Telescopes and Instrumentation for Solar Astrophysics*, Stephen L. Keil, Sergey V. Avakyan, ed., Proc. SPIE **4853**, 370-380 (2003).
 - [12] C. U. Keller, Claude Plymate, and S. M. Ammons, “Low-cost solar adaptive optics in the infrared” Proc. SPIE **4853**, in *Innovative Telescopes and Instrumentation for Solar Astrophysics*, Stephen L. Keil, Sergey V. Avakyan, ed., 351-359 (2003).
 - [13] Frequently asked questions-OKOTECH, <http://www.okotech.com/howtobiasthemmdm>.
 - [14] OKO Technologies, 37(19)-Channel micromachined deformable mirror system: technical passport
 - [15] ZEMAX Development Corporation, 3001 112th Avenue NE, Suite 202, Bellevue, WA 98004-8017 USA.
 - [16] R. J. Noll, “Zernike polynomial and atmospheric turbulence”, J. Opt. Soc. Am. **66**, 207-211 (1976).
 - [17] ZEMAX User’s guide, “Surface types”, chapter 11, page 308. 25, June (2007).
 - [18] A. E. H. Love, “A treatise on the mathematical theory of elasticity”, Chapter 22, Dover publications, NewYork, (2007).

- [19] A. Gómez-Vieyra and D. Malacara-Hernández, “Geometric theory of wavefront aberrations in an off-axis spherical mirror, *Appl. Opt.* **50**, 66-73, 2011